JOURNAL OF MATERIALS SCIENCE 22 (1987) 4460–4464

The surface diffusion coefficients of MgO and Al_2O_3

P. ŠAJGALÍK, Z. PÁNEK, M. UHRÍK
Institute of Inorganic Chemistry, Centre for Chemical Research, Slovak Academy of Sciences, Dúbravská cesta 9, CS-842 36 Bratislava, Czechoslovakia

From the measurement of neck size and neck curvature during the sintering of two spheres the surface diffusion coefficients of MgO and Al_2O_3 were determined. The spheres of both materials were machined from single crystals. The following values of surface diffusion coefficients were found: for MgO, $D_s\delta_s = 3.7 \times 10^{-4} \exp(407.8\,\mathrm{kJ\,mol^{-1}}/RT)\ \mathrm{m^3\,sec^{-1}}$; for Al_2O_3, $D_s\delta_s = 1.5 \times 10^{-2} \exp(518.7\,\mathrm{kJ\,mol^{-1}}/RT)\ \mathrm{m^3\,sec^{-1}}$.

1. Introduction

Most ceramic bodies are fabricated by sintering. One of the aims in ceramic technology is the achievement of a certain relative density of the final product. To accomplish this, a knowledge of the diffusion data of particular materials is desirable. Mass transport to the necks by surface diffusion is not accompanied by densification of the sintering powder compact. That is the reason why the rate of surface diffusion is studied in connection with sintering processes.

The rate of the sintering process is often used for determination of diffusion data [1–6]. This method gives reliable results only if (i) the conditions of the experiment guarantee the absolute dominancy of the particular diffusion, and (ii) the equation used for calculation of the respective material property fully represents the experimental model used.

These two conditions are not always fulfilled in the determination of surface diffusion coefficients from sintering data. Sintering experiments with two spheres under certain experimental conditions which guarantee the dominancy of the particular sintering mechanisms can overcome the problems mentioned above.

2. Procedure for surface diffusion coefficient calculation

Sintering maps are useful aids in the determination of the dominant mechanism during sintering, provided all the necessary material characteristics are known [7, 8]. The map for a given sintering temperature, time and particle size (for a two-particle model) depicts the neck size and simultaneously determines the regions of dominancy of individual sintering mechanisms. The area of the diagram, limited by the coordinates log (x/a) and T/T_M (x is the neck radius, a is the spherical particle radius, T is the sintering temperature and T_M is the melting temperature of the material) is divided into fields. Each field represents the mechanism contributing dominantly to the neck growth. Using the procedure suggested by Šajgalík *et al.* [9], it is possible to specify the areas on the map where the contribution of the particular sintering mechanism is exceeding some given value, e.g. 99%.

Figs 1 and 2 show such maps for two spheres of MgO and Al_2O_3, respectively. The material constants listed in Tables I and II were used in the construction of the sintering maps. The region limited by a dashed line facing the higher temperatures, represents a more than 99% contribution of surface diffusion to neck growth. The contributions of other mass transport mechanisms are negligible within this area. If the conditions of the sintering experiment (particle radii, sintering temperature and time) are set according to the requirement of more than 99% of surface diffusion, then the kinetics of neck growth between the spheres can be expressed by the following equation [7]:

$$\frac{\dot{x}_{tot}}{a} = \frac{2D_s\delta_s}{a^4}\frac{\gamma\Omega}{kT}(aC)^3 \qquad (1)$$

where D_s is the surface diffusion coefficient, δ_s is the surface thickness where surface diffusion occurs, γ is the square density of the Gibbs energy, Ω is the volume of the diffusing particle, k is Boltzmann's constant, $\dot{x}_{tot}$ is the rate of neck growth and C is the curvature difference between the positions of the source and sink of matter flux. C can be expressed as

$$C = \frac{2}{a} - \left(\frac{1}{x} - \frac{1}{\varrho}\right) \qquad (2)$$

where x is the neck radius and ϱ is the radius of the neck curvature. The curvature difference C is responsible for a concentration gradient of vacancies, according to the Kelvin equation. Material flow to the neck region (neck growth) at elevated temperatures is the consequence of this gradient. The function $C = C(t)$ can be obtained by measuring the values of x and ϱ during the sintering run. Thus, the only unknown constant in Equation 1 is the surface diffusion coefficient $D_s\delta_s$. The surface diffusion coefficient determined in this paper includes the value δ_s, and both values (D_s and δ_s) together represent one material characteristic, marked as $D_s\delta_s$.

3. Experimental procedure

The evolution of the neck during sintering was

0022–2461/87 $03.00 + .12 © 1987 Chapman and Hall Ltd.

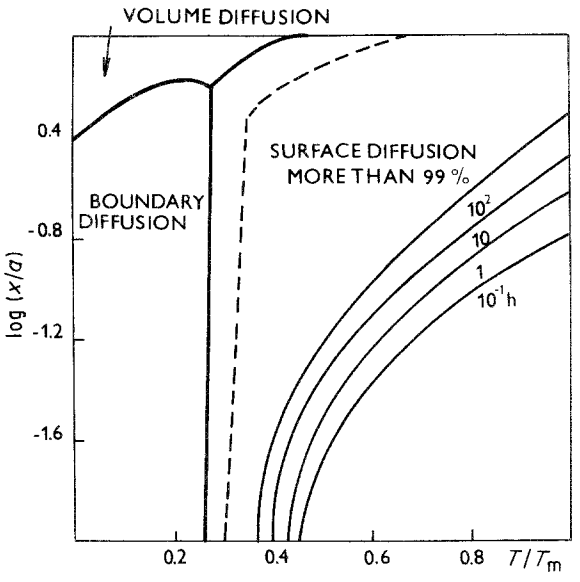

Figure 1 Sintering map for two spheres of MgO. Radii of spheres are 2.2×10^{-4} m.

observed in a heating microscope. Single crystals of MgO and Al_2O_3 were used for the preparation of the spheres. Spectral analyses of the materials studied are in Tables III and IV. The sample holder was made of the same type of material as the spheres under study. The sintering experiments were performed under isothermal conditions. The sizes of spheres, sintering time and temperature were set to fulfil the condition of dominancy of surface diffusion according to the sintering maps (Figs 1 and 2). The radii of the spheres were 2.2×10^{-4} m for MgO and 1.7×10^{-4} m for Al_2O_3. Sintering temperatures were 1450, 1500 and 1600° C for MgO and 1400, 1550 and 1600° C for Al_2O_3. According to the sintering maps, which were calculated for the sphere radii used in the experiments, surface diffusion is dominant also at lower temperatures, but there are two reasons to select them relatively high:

(i) the duration of the sintering process would be extremely long at lower temperatures, and

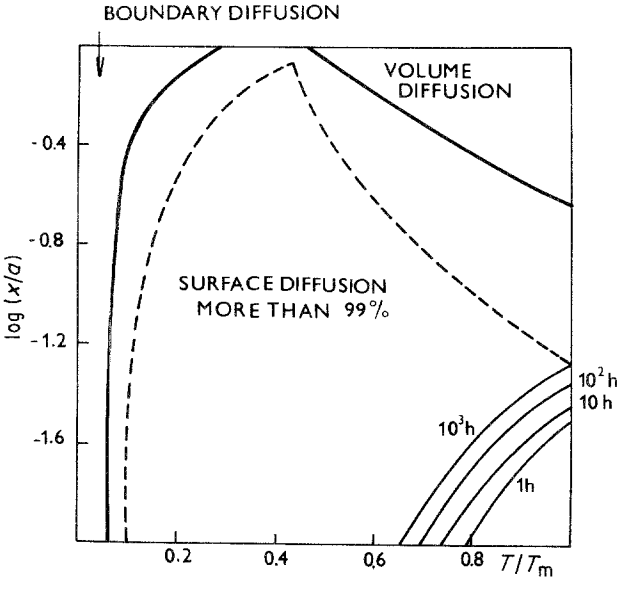

Figure 2 Sintering map for two spheres of Al_2O_3. Radii of spheres are 1.7×10^{-4} m.

TABLE I Material constants of MgO used in the construction of the sintering map

Volume of diffusing particle, Ω	1.87×10^{-29} m^3	[10]
Melting temperature, T_M	3125 K	[10]
Pre-exponential for lattice diffusion, D_{ov}	2.5×10^{-10} m^2 sec^{-1}	[10]
Activation energy for lattice diffusion, Q_v	261.3 kJ mol^{-1}	[10]
Pre-exponential for boundary diffusion, $D_{ob}\delta_b$	2.5×10^{-17} m^3 sec^{-1}	*
Activation energy for boundary diffusion, Q_b	172.5 kJ mol^{-1}	[10]
Pre-exponential for surface diffusion, $D_{os}\delta_s$	2.3×10^{-6} m^3 sec^{-1}	†
Activation energy for surface diffusion, Q_s	376.8 kJ mol^{-1}	[11]
Surface density of Gibbs energy, γ	1 J m^{-2}	[12]
Theoretical density, Δ_0	3.58×10^3 kg m^3	[12]
Pre-exponential for vaporization, P_0	1.75×10^9 MPa	[12]
Activation energy for vaporization, Q_{vap}	0.5 kJ mol^{-1}	[12]

*D_{ob} from [10]; δ_b inferred from data for materials of the same structure and comparable melting point as $\delta_b \simeq 10^{-7}$ m.
†D_{os} from [11]; δ_s the same as δ_b above.

(ii) the sintering maps were constructed using literature values for material constants. Some of these were only estimates and those determined experimentally were measured on different materials. If the values of boundary and volume diffusion coefficients used in constructing the sintering maps were higher, the region of the surface diffusion would be smaller [17]. The relatively higher sintering temperatures ensure surface diffusion dominancy also in the case when the material data used were slightly different.

No centre-to-centre approach of the spheres was observed. During the sintering process the neck growth was accompanied by the creation of an undercut region in the vicinity of the neck, shown by arrow in Fig. 3. Both observed phenomena indicate the dominancy of surface diffusion.

TABLE II Material constants of Al_2O_3 used in the construction of the sintering map

Volume of diffusing particle, Ω	2.11×10^{-29} m^3	[6]
Melting temperature, T_M	2325 K	[13]
Pre-exponential for lattice diffusion, D_{ov}	0.19 m^2 sec^{-1}	[14]
Activation energy for lattice diffusion, Q_v	636.4 kJ mol^{-1}	[14]
Pre-exponential for boundary diffusion, $D_{ob}\delta_b$	2.0×10^{-11} m^3 sec^{-1}	*
Activation energy for boundary diffusion, Q_b	460.5 kJ mol^{-1}	[15]
Pre-exponential for surface diffusion, $D_{os}\delta_s$	2.83×10^{-8} m^3 sec^{-1}	[6]
Activation energy for surface diffusion, Q_s	477.3 kJ mol^{-1}	[6]
Surface density of Gibbs energy, γ	0.9 J m^{-2}	[6]
Theoretical density, Δ_0	3.97×10^3 kg m^3	[6]
Pre-exponential for vaporization, P_0	1.66×10^{13} Pa	[16]
Activation energy for vaporization, Q_{vap}	540.1 kJ mol^{-1}	[16]

*D_{ob} from [15]; δ_b inferred from data for materials of the same structure and melting point, $\delta_b \simeq 10^{-7}$ m.

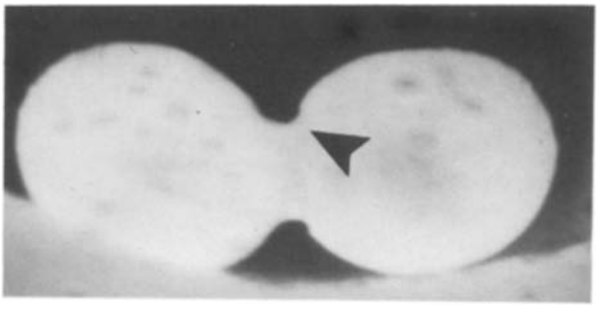

Figure 3 Effect of undercutting on neck curvature. Two spheres of MgO single crystal (radius 2.2×10^{-4} m) sintered 145 h at 1550° C.

Two Type B thermocouples were used for temperature measurement and control. The temperature was controlled with an accuracy ± 5 K. Sintering spheres were photographed at particular time intervals (Figs 4 and 5). Fig. 4 shows sintering MgO spheres at 1500° C after 50, 143 and 213 h and Fig. 5 shows Al_2O_3 spheres at 1550° C after 119, 183 and 206 h. Values of x and ϱ were measured on enlarged photographs and from these data the function $C = C(t)$ was constructed according to Equation 2. In the case of $(x/a) < 0.1$ the approximate formula [18]

$$\frac{\varrho}{a} \simeq 0.26 \left(\frac{x}{a}\right)^{4/3} \tag{3}$$

was used for determination of the ϱ value.

4. Surface diffusion coefficients of MgO and Al_2O_3 single crystals

Figs 6 and 7 show the log $(\dot{x}/a)$ against log (aC) curves at different temperatures for MgO and Al_2O_3 single crystals. The experimental results were approximated by least-square fittings as follows:

$$\begin{aligned} \text{MgO: } 1450^\circ\text{C} \quad & \log(\dot{x}/a) = 2.95 \log(aC) - 10.06 \\ 1500^\circ\text{C} \quad & \log(\dot{x}/a) = 3.09 \log(aC) - 9.70 \\ 1600^\circ\text{C} \quad & \log(\dot{x}/a) = 3.00 \log(aC) - 9.19 \end{aligned} \tag{4}$$

$$\begin{aligned} \text{Al}_2\text{O}_3\text{: } 1400^\circ\text{C} \quad & \log(\dot{x}/a) = 3.03 \log(aC) - 11.70 \\ 1550^\circ\text{C} \quad & \log(\dot{x}/a) = 2.97 \log(aC) - 10.51 \\ 1600^\circ\text{C} \quad & \log(\dot{x}/a) = 3.05 \log(aC) - 9.98 \end{aligned} \tag{5}$$

The surface diffusion coefficients, calculated according to Equations 1, 4 and 5 are listed in Table V. The folowing γ and Ω values were used during the calculation:

$$\begin{aligned} \text{MgO: } \gamma &= (1.2 \text{ to } 2.8 \times 10^{-4} T)\,\text{J mol}^{-1} \text{ [19]} \\ \Omega &= 1.86 \times 10^{-29}\,\text{m}^3 \text{ [10]} \end{aligned}$$

TABLE III Spectral analysis of MgO single crystal

Element	Concentration (wt %)
Mg	Main element
Al	0.1 to 0.5
Fe	0.1 to 0.5
Si	0.05 to 0.1
Ca	0.05 to 0.1
B	0.01 to 0.05
Cr	0.01 to 0.05
Mn	0.005 to 0.01
Cu	0.001 to 0.005

TABLE IV Spectral analysis of Al_2O_3 single crystal

Element	Concentration (wt %)
Al	Main element
Fe	0.05 to 0.1
B	0.01 to 0.05
Mg	0.005 to 0.01
Ca	0.005 to 0.01
Mn	0.001 to 0.005
Cu	0.001 to 0.005

$$\begin{aligned} \text{Al}_2\text{O}_3\text{: } \gamma &= 0.9\,\text{J mol}^{-1} \text{ [6]} \\ \Omega &= 2.11 \times 10^{-29}\,\text{m}^3 \text{ [6]} \end{aligned}$$

The surface diffusion coefficients for MgO and Al_2O_3 are shown in Fig. 8. The present values for MgO and Al_2O_3 are marked as 1 and 6, respectively. Robertson [11] measured the surface diffusion coefficient of MgO by a thermal grooving method, marked as 2 on Fig. 8. These results are approximately one order of magnitude lower than the present ones. The difference can be expressed by a higher content of impurities in the MgO single crystals used in the present experiments. Line 3 represents the results of Robertson and Chang [20] for Al_2O_3 and Line 4 those of Kitazawa *et al.* [21], obtained by a surface flattening method. The present results for Al_2O_3 are of the same order as these and some other results [10, 22, 23]. Surface diffusion coefficients obtained from the sintering data [2, 3, 5, 6] are on Fig. 8 represented by Komatsu's results, marked as 5 [6]. All these results differ by a few orders of magnitude from the set of results mentioned above. The difference indicates a possibility that some of the conditions mentioned in the introduction were not fulfilled during the determination of surface diffusion coefficients from the sintering data.

A problem can arise during the application of the present procedure when the surface diffusion coefficient used for constructing the sintering map deviates substantially from the right one. Thus, the

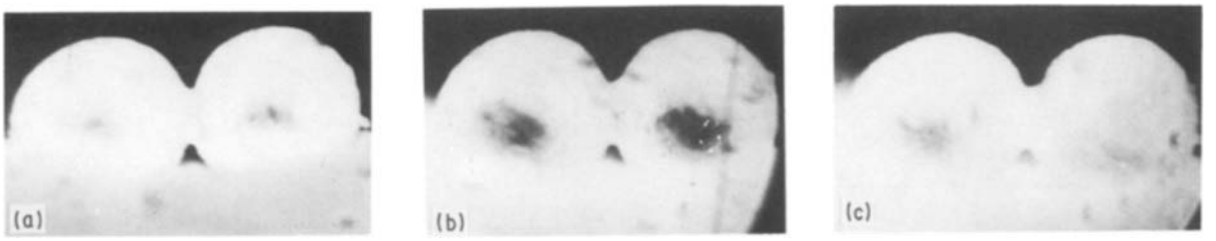

Figure 4 Spheres of MgO single crystal sintered at 1500° C for (a) 50 h, (b) 143 h and (c) 213 h. Radii of spheres are 2.2×10^{-4} m.

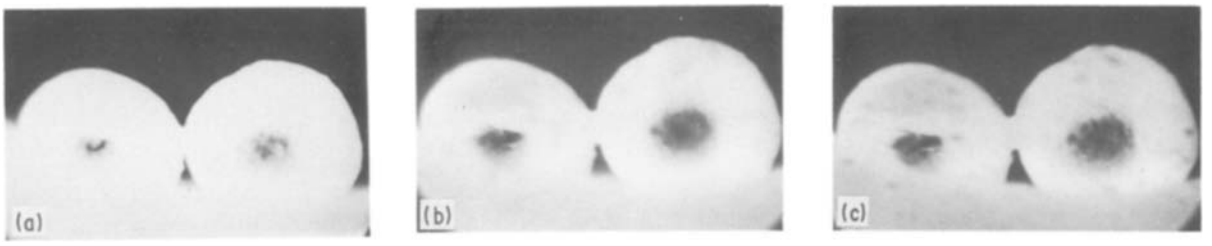

Figure 5 Spheres of α-Al_2O_3 single crystal sintered at 1550° C for (a) 119 h, (b) 183 h and (c) 206 h. Radii of spheres are 1.7×10^{-4} m.

experimental conditions selected according to the calculated sintering map can lie outside the region of surface diffusion dominancy. In this case, the surface diffusion coefficient obtained is set for the calculation of a new map and a new model experiment is carried out. This cycle is repeated until surface diffusion dominancy is proved by experiment (no centre-to-centre approach or undercutting in the vicinity of the neck, etc.).

5. Conclusions

Sintering maps offer a possibility for finding the experimental conditions where surface diffusion is the dominant sintering mechanism.

A model experiment (sintering a pair of spheres) gives a possibility of achieving the conditions resulting from the map.

The surface diffusion coefficients obtained in the present paper are as follows:-

$$\text{MgO:}\quad D_s\delta_s = 3.7 \times 10^{-4} \times \exp\left(\frac{407.8\,\text{kJ mol}^{-1}}{RT}\right) \text{m}^3\text{sec}^{-1}$$

$$Al_2O_3\text{:}\quad D_s\delta_s = 1.5 \times 10^{-2} \times \exp\left(\frac{518.7\,\text{kJ mol}^{-1}}{RT}\right) \text{m}^3\,\text{sec}^{-1}$$

These results are in good agreement with the results obtained by different methods.

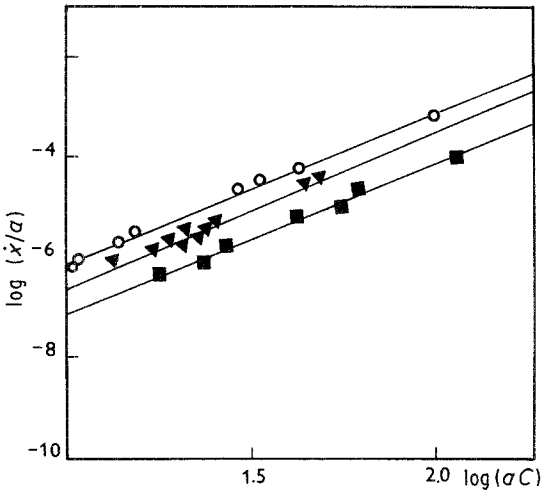

Figure 6 The log $(\dot{x}/a)$ against log (aC) dependences measured on MgO spheres sintered at (■) 1450° C (▼) 1500° C and (○) 1600° C.

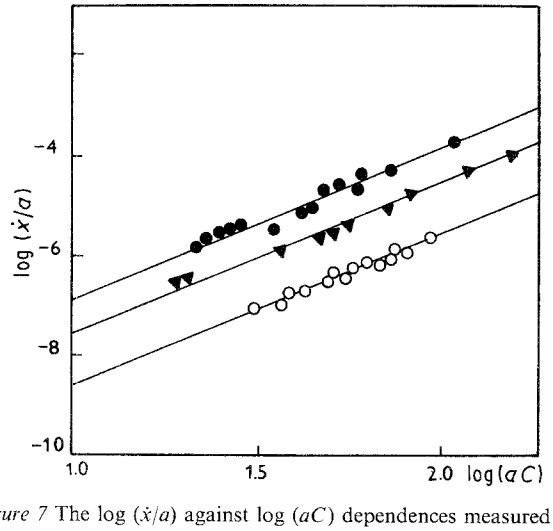

Figure 7 The log $(\dot{x}/a)$ against log (aC) dependences measured on Al_2O_3 spheres sintered at (○) 1400° C, (▼) 1550° C and (●) 1600° C.

TABLE V Surface diffusion coefficients for MgO and Al_2O_3 single crystals

MgO		Al_2O_3	
T (° C)	$D_s\delta_s$ (m^3 sec^{-1})	T (° C)	$D_s\delta_s$ (m^3 sec^{-1})
1450	1.98×10^{-16}	1400	1.03×10^{-18}
1500	4.80×10^{-16}	1550	1.74×10^{-17}
1600	1.50×10^{-15}	1600	5.92×10^{-17}

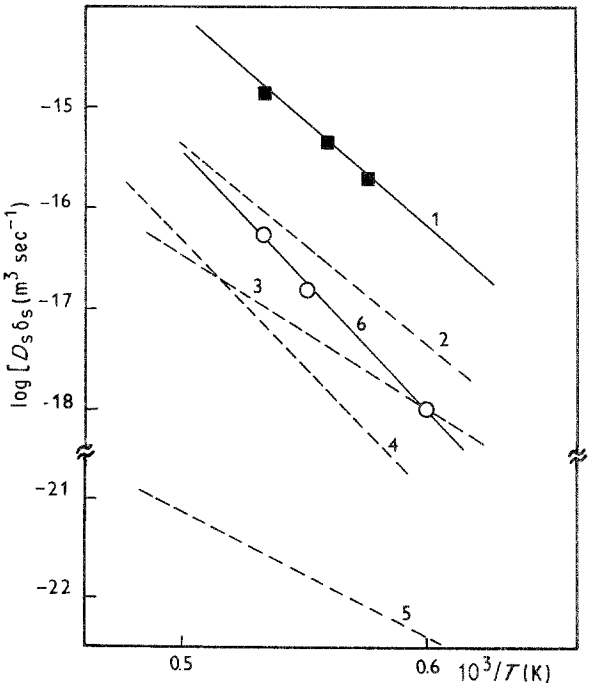

Figure 8 Surface diffusion coefficients for MgO and Al_2O_3. MgO: (1) this work, (2) thermal grooving [11]. Al_2O_3: (3) thermal grooving [20], (4) surface flattening [21], (5) sintering of powder compact [6], (6) this work. The surface diffusion coefficients for (2) to (5) include the value $\delta_s = 10^{-7}$ m.

Acknowledgement

The authors wish to express their thanks to Dr M. Haviar for valuable discussions.

References

1. G. C. KUCZYNSKI, *Trans. AIME* **185** (1949) 169.
2. W. R. RAO and I. B. CUTLER, *J. Amer. Ceram. Soc.* **55** (1972) 170.
3. Y. MORIYOSHI and W. KOMATSU, *Yogyo-Kyokai-Shi* **81** (1973) 102.
4. *Idem, ibid.* **84** (1976) 348.
5. S. PROCHAZKA and R. L. COBLE, *Phys. Sintering* **2** (1970) 1.
6. W. KOMATSU, Y. MORIYOSHI, S. K. MOON, H. KAMATA and S. KURASHIMA, *Yogyo-Kyokai-Shi* **85** (1977) 185.
7. M. F. ASHBY, *Acta Metall.* **22** (1974) 275.
8. F. B. SWINKELS and M. F. ASHBY, *Powder Metall.* **1** (1980) 1.
9. P. ŠAJGALÍK, M. HAVIAR and Z. PÁNEK, *Z. Metallkde* **77** (1986) 193.
10. M. F. ASHBY, *Acta Metall.* **20** (1972) 887.
11. W. M. ROBERTSON, in "Sintering and Related Phenomena", edited by G. C. Kuczynski, N. A. Hooton and C. F. Gibbon (Gordon and Breach, New York, 1967) p. 215.
12. E. RYSHKEWITCH, "Oxide Ceramics" (Academic, New York, 1960) pp. 279–287.
13. E. DÖRRE and H. HÜBNER, "Aluminia" (Springer, Berlin, 1984) p. 12.
14. M. O'KEEFE, in "Sintering and Related Phenomena", edited by G. C. Kuczynski, N. A. Hooton and C. F. Gibbon (Gordon and Breach, New York, 1967) p. 57.
15. Y. OISHI, W. D. KINGERY, *J. Chem. Phys.* **33** (1960) 480.
16. R. C. WEAST (ed.), "Handbook of Chemistry and Physics" (Chemical Rubber Co., Cleveland, 1970) p. D-166.
17. V. SMOLEJ, *Z. Metallkde* **74** (1983) 689.
18. W. S. COBLENZ, J. M. DYNYS, R. M. CANNON and R. L. COBLE, in "Sintering Processes", edited by G. C. Kuczynski (Plenum, New York, 1980) p. 141.
19. S. K. RHEE, *Mater. Sci. Eng.* **11** (1973) 311.
20. W. M. ROBERTSON and R. CHANG, in "The Role of Grain Boundaries and Surfaces in Ceramics", edited by W. W. Kriegel and H. Palmour III (Plenum, New York, 1966) p. 49.
21. K. KITAZAWA, I. KOMAKI, K. FUEKI and T. MUKAIBO, in Proceedings of 14th Annual Meeting on Basic Science of Ceramics, January 1976.
22. J. F. SHACKELFORD and W. D. SCOTT, *J. Amer. Ceram. Soc.* **51** (1968) 688.
23. R. L. COBLE and C. F. YEN, *ibid.* **55** (1972) 507.

Received 23 February
and accepted 28 April 1987